# ANALYSIS OF OTFS AND ITS COMPARISON WITH PRE-CODED MC-CDMA WITH CHANNEL ESTIMATION AND TARGET CLASSIFICATION IN A DISTRIBUTED RADAR SYSTEM

*A project report*
*submitted by*

**KOLLIBOINA SAI TEJA**

*in partial fulfilment of the requirements*
*for the award of the dual degree of*

**BACHELOR OF TECHNOLOGY**
**and**
**MASTER OF TECHNOLOGY**


**DEPARTMENT OF ELECTRICAL ENGINEERING**
**INDIAN INSTITUTE OF TECHNOLOGY MADRAS**
**JUNE 2022**

# THESIS CERTIFICATE

This is to undertake that the Thesis titled **ANALYSIS OF OTFS AND ITS COMPARISON WITH PRE-CODED MC-CDMA WITH CHANNEL ESTIMATION AND TARGET CLASSIFICATION IN DISTRIBUTED RADAR SYSTEM**, submitted by **K Sai Teja(EE17B046)** to the Indian Institute of Technology Madras, for the award of **Bachelor of Technology and Master of Technology**, is a bona fide record of the research work done by him under the supervision of **Dr K Giridhar**. The contents of this Thesis, in full or in parts, have not been submitted to any other Institute or University for the award of any degree or diploma.

**Chennai 600036**

**Date: June 2022**

**Prof. K Giridhar**
Project Guide
Professor
Department of Electrical Engineering
IIT Madras, 600036

## ACKNOWLEDGEMENT

At the outset, I would like to express my sincere gratitude to my project guide Prof. K Giridhar who has kindly accepted my request to join his research team for which I feel deeply honoured and indebted to him, who with his vast years of experience and expertise has provided me immense guidance and support throughout the course of the project.

I am ever grateful to Sruti S, PhD Research Scholar working under Prof. K Giridhar, for guiding me and motivating me at every step throughout the project. I would like to take this opportunity to thank all my professors at IIT Madras who have imparted knowledge and motivated me to learn the intricacies of the subject. I am thankful to all my friends who stood by me and supported me in all my endeavours. Last but not the least, I would like to thank my parents who played a major role in moulding my career without whom I would not have been in this position.

# Contents

# List of Figures

## List of Tables

# Abstract

Embedded pilot aided channel estimation for Orthogonal Time Frequency Space (OTFS) modulation in Delay-Doppler domain is shown to have similar error performance when compared with ideally known channels. This study analyses how OTFS performance varies with different values of M and N. This study also investigates how OTFS compares to Orthogonal Frequency Division Multiplexing (OFDM) and various Multi-Carrier Code Division Multiple Access (MC-CDMA) schemes. Extended Vehicular - A (EVA) channel is used for comparing the above schemes. Different ways of power allocation to pilots and data symbols for MC-CDMA and OFDM is implemented to match the pilot power in OTFS. Same amount of overhead and average power transmitted per symbol are maintained constant for fair comparison among the schemes. Our work shows that the bit error performance of OTFS improves as M and N increases. For a constant M*N, OTFS performs well when both M and N are maximised. The impact of Peak to Average Power Ratio (PAPR) is captured in the effective SNR. MC-CDMA outperforms OTFS with channel estimation in almost all scenarios due to the privilege that MC-CDMA schemes get better SNR for data symbols compared to OTFS when both the schemes have the same transmit power.

Bistatic Radar Cross Section (RCS) signatures for different objects are different. It can be used to identify the type of target. This work studies about using bistatic RCS of targets to classify whether it is a quadcopter or a fixed-wing drone. In this work, Bistatic RCS of two quadcopters and two fixed-wing drones are computed using Ansys HFSS software. The bistatic RCS of targets are computed from the received radar signals at the receivers in a Multi-static radar system. Two metrics are proposed to classify the target based on the calculated bistatic RCS. Similarity metric finds how close the target's bistatic RCS to a typical quadcopter and a fixed-wing drone is by measuring the distance from each. Symmetric metric calculates the error from bistatic RCS by exploiting the fact of having different types of symmetry for the two types of drones. Our analysis shows that both metrics were able to identify the type of target based on its received signature.

# ANALYSIS OF OTFS AND ITS COMPARISON WITH PRE-CODED MC-CDMA WITH CHANNEL ESTIMATION

## 2.1 Introduction

### 2.1.1 Motivation

One of the goals of future communication systems is to have reliable communications in high mobility situations like vehicle to vehicle communications, in high speed trains. Currently OFDM is dominantly used modulation technique that is used in 4G. In high mobility scenario, OFDM experiences significant degrade in performance due to Doppler spread of time varying channels. This Doppler spread will cause Inter Carrier Interference (ICI) which in turn degrades OFDM's performance. Many techniques have been explored to get better performance in presence of Doppler spread. Orthogonal Time Frequency Space (OTFS) modulation is one such technique that is said to give better performance than OFDM systems by exploiting channel representation in Delay-Doppler domain.
The aim of this thesis is study how performance of OTFS with pilot aided channel estimation compares with other popular schemes like OFDM, MCCDMA with different types of spreading in different scenarios, analyse the PAPR of the schemes and develop an adaptive thresholding scheme independent of channel statistics and noise variance.

## 2.2 Modulation Schemes

In this thesis, we have compared performance of four different schemes. They are OTFS, MCCDMA-FS (Frequency spread), MCCDMA-TFS (Time Frequency spread) and OFDM. Above all schemes are multi carrier modulation techniques.

In the following scenarios,
$X$ = input data symbol matrix of size M*N
$Y$ = received data symbol matrix of size M*N
h(t,$\tau$) = channel
H = channel matrix of size M*N represented in time-frequency domain
$H_2$ = channel matrix represented in Delay-Doppler domain.
$F_M$ = FFT matrix of size M
$F_N$ = FFT matrix of size N

### 2.2.1 OFDM

Orthogonal Frequency Division Multiplexing (OFDM) is a type of data transmission where data is encoded to multiple narrow band subcarriers. Modulated data is placed in frequency domain. Each subcarrier acts as an independent narrowband channel for that input data symbol.

Figure 1 shows the implementation of OFDM systems. The input symbols are converted to time domain from frequency domain by using Inverse Discrete Fourier Transform. Cyclic prefix is used to make linear convolution look like circular convolution. After transmitting through the channel, the received symbols are again moved back to frequency domain and demodulated to get the bits received.

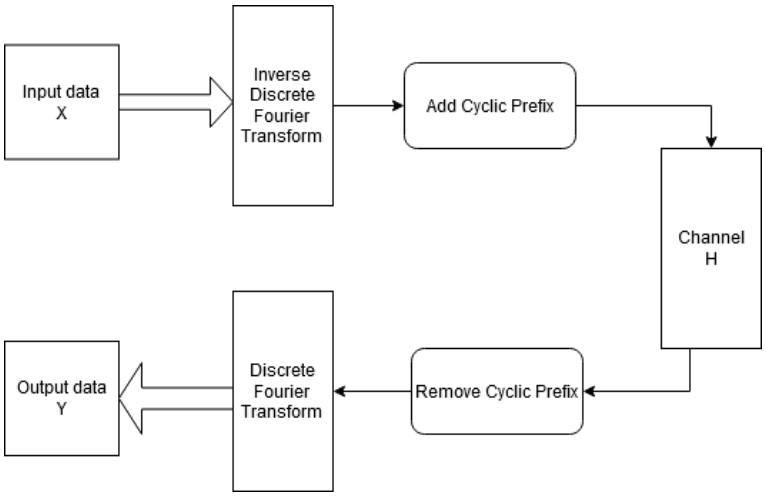


Figure 1: OFDM implementation block diagram

The input-output relation in OFDM for a resource grid of size M*N is in the absence of Doppler shift is

$$Y[m,n] = H[m,n]X[m,n] + noise$$

where
$m = 1, 2, ..M$ and $n = 1, 2, ..N$
M = number of subcarriers
N = number of OFDM symbols

OFDM does not work properly when there is Doppler spread in the channel as it shifts the subcarriers thus making them lose their orthogonality.

### 2.2.2 MC-CDMA

This technique is a combination of OFDM and spread spectrum techniques. In this technique, different users share same bandwidth and same timeslot. These users use different codes, which are used to separate each user data from common data. MC-CDMA transmits data of single user in all subcarriers. This is implanted as an OFDM block

with a spreading block before and a de-spreading block after the OFDM block.
The data symbols are spread using different types of codes. The spread data chips are mapped in frequency dimension or in time dimension or in both dimensions. In this work, mapping across Frequency (FS) and mapping across both Time and Frequency (TFS) are considered.

Figure 2 shows the MC-CDMA implementation.

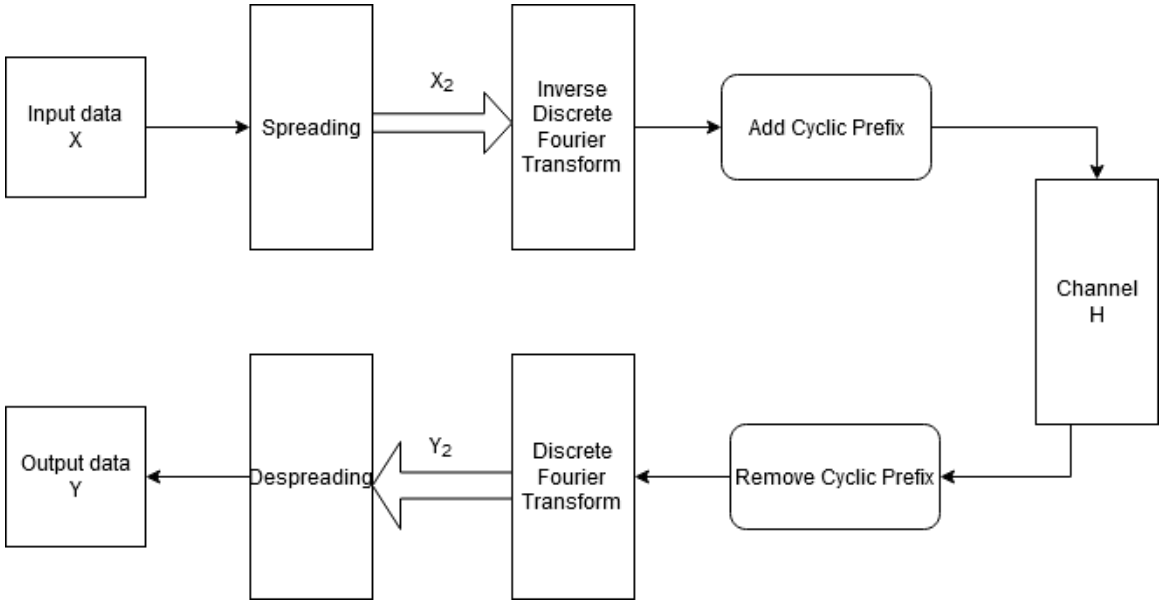


Figure 2: MC-CDMA implementation block diagram

Let $X_2$ be the data matrix of size M*N after spreading. After transmitting the spreaded data symbols in an OFDM system, let $Y_2$ be the symbols received at the receiver. After passing the received data through an equaliser, they are despreaded. The input-output relations among these matrices are as follows.

$$X_2 = spreading(X)$$

$$\mathrm{Y}_2[m,n] = H[m,n]X_2[m,n] + noise \quad \text{n = 1,2,...N and m= 1,2,...M}$$

$$\mathrm{Y}_3 = Equaliser(Y_2)$$
$$\mathrm{Y} = \mathrm{despreading}(\mathrm{Y}_3)$$

**Spreading Codes**
There exist many codes to spread data. The selection of spreading code depends on some properties like orthogonality, PAPR, complexity, etc. In this work, we used two types of spreading codes. They are Walsh – Hadamard Codes and Zadoff- Chu codes.

**Walsh-Hadamard Codes** These codes are orthogonal. These are generated according to this formula.

$$C_L = \begin{bmatrix} C_{\frac{L}{2}} & C_{\frac{L}{2}} \\ C_{\frac{L}{2}} & -C_{\frac{L}{2}} \end{bmatrix}, \quad \forall L = 2^m \quad m \geq 1, \quad C_1 = 1$$

The length of the Walsh-Hadamard codes is always in the form of powers of 2.

**Zadoff-Chu codes**
Zadoff-chu codes are not orthogonal. They are generated by cyclical shifting of the first sequence. Even if they are not orthogonal, their cross-correlation magnitude is very small and hence are called as pseudo orthogonal codes. These are generated by this formula.

$$c_l^{(k)} = \begin{cases} e^{j2\pi k(ql+\frac{l^2}{2})/L} & \text{for L even} \\ e^{j2\pi k(ql+\frac{l^2+l}{2})/L} & \text{for L odd} \end{cases}$$

where $q$ is any integer and $k$ is an integer, prime with $L$. If $L$ is a prime number, a set of Zadoff–Chu codes is composed of $L-1$ sequences. The complete set of codes are generated by cyclic shifting the above sequence.

### 2.2.3 OTFS

OTFS is a modulation scheme where data symbols are placed across Delay-Doppler domain. Delay-Doppler channel representation is used because, the channel variation in Delay and Doppler is very small when compared to its variation in time-frequency domain even in high mobility scenario. OTFS can also be implemented as a cascaded system of data preprocessing block and OFDM block and postprocessing blocks. The symbols placed in Delay Doppler domain are transformed to time-frequency domain and are transmitted through OFDM modulation. At the receiver the data is again transformed back to Delay-Doppler domain. These transforms are called Symplectic Finite Fourier Transforms.

The Symplectic transforms spread each data symbol in Delay-Doppler domain to an entire resource grid in time-frequency domain orthogonally. So, OTFS can also be viewed as a type of MC-CDMA with Symplectic transform as its spreading code. Figure 3 shows practical OTFS implementation.

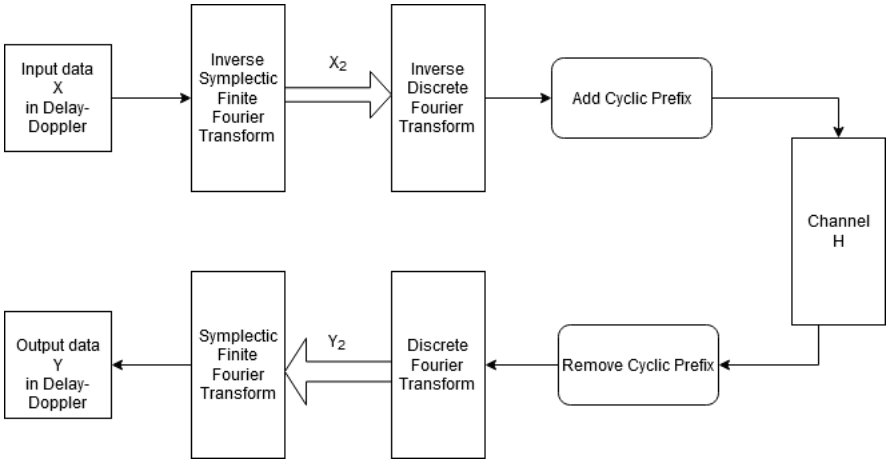


Figure 3: OTFS implementation block diagram

The input-output relation for OTFS is as follows.

$$Y_2[n,m] = H[n,m]X_2[n,m] + noise$$
$$\text{H[n,m]} = \iint e^{-j2\pi\nu\tau} h(\nu,\tau) e^{-j2\pi(m\tau - nT\nu)}\, d\tau\, d\nu$$
$$\text{Y} = \text{Circ2D}(\text{H}_2, X) + noise$$

where Circ2D represents 2-dimensional circular convolution of the two matrices.

## 2.3 Pilot Aided Channel Estimation

Pilots are the known symbols that are sent along with data symbols to estimate the channel at the receiver. As number of pilots increases, the accuracy of channel estimation increases but the throughput decreases. There is a trade-off between number of pilots that can be used and throughput of the communication system.
In this work, OTFS with pilot aided channel estimation is compared with other available schemes.

### 2.3.1 OFDM

In OFDM resource grid, pilots can be placed in many ways. In this work, pilots are placed evenly for every OFDM symbol. In this scenario, channel estimation is done for every OFDM symbol. Figure 4 shows the pilot structure for OFDM.
If P is the pilot placed, the channel frequency response for the subcarriers where pilots are placed can be known.

$$H[m_p, n_p] = \frac{Y[m_p, n_p]}{P}$$

where $m_p, n_p$ are the indices where pilot is placed.
The channel frequency response for other subcarriers is estimated by

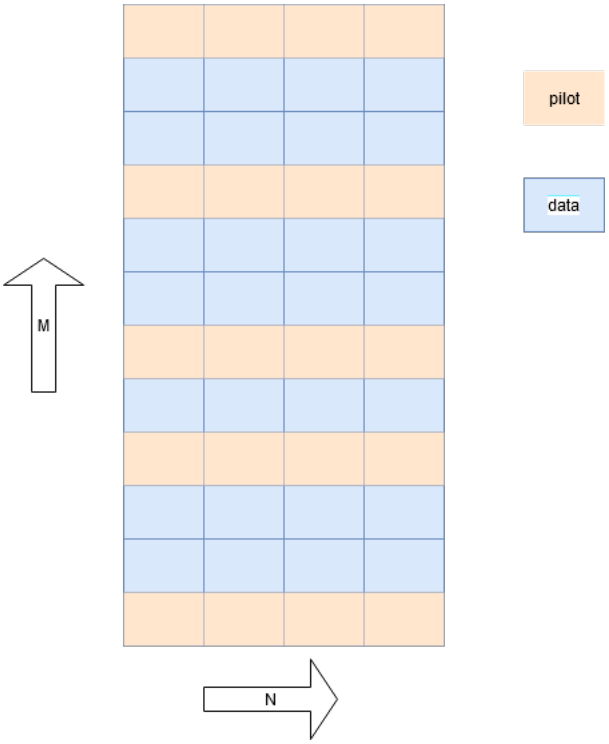


Figure 4: Arrangement of symbols for OFDM and MC-CDMA[1]

interpolating the response of the subcarriers carrying pilots. In this work, spline interpolation is used. The received data is equalised after channel response is estimated.

### 2.3.2 MC-CDMA

MC-CDMA is implemented as OFDM system with spreading and despreading blocks. In this work, MC-CDMA used the same embedded pilot structure as of OFDM[1]. Input data is spreaded using a spreading code and placed across the time frequency resource grid and transmitted. At the receiver, the received data is equalised and despreaded.

### 2.3.3 OTFS

In this work, the channel estimation is done in Delay-Doppler domain[2], where as in other schemes, channel estimation is done in time-frequency domain. The main idea behind this method is the input-output relation of data with channel in Delay-Doppler dimension.

$$Y = Circ2D(H_2, X) + noise$$

where Circ2D represents 2-dimensional circular convolution of two matrices.
In this method, input data symbols, guard symbols and a single pilot are placed in such a way that received symbols in Delay-Doppler domain contains the channel matrix. Figure 5 shows the structure of resource grid of transmitted symbols and received symbols in Delay-Doppler domain.

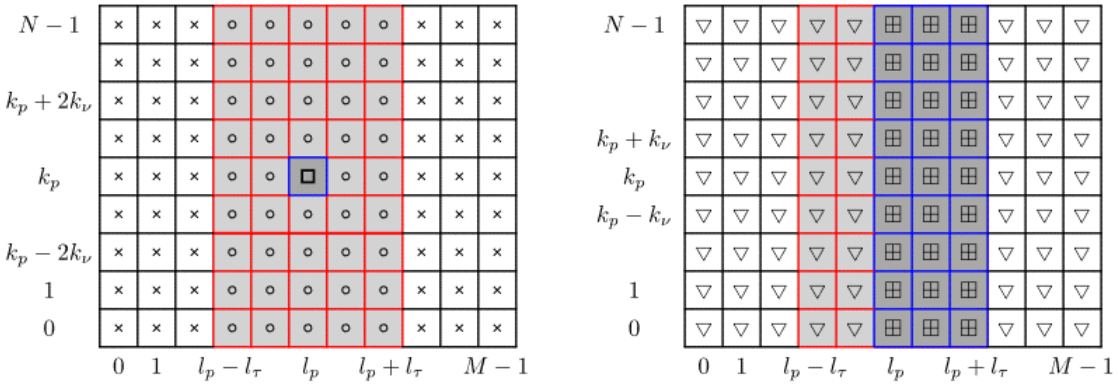


(a) Tx symbol arrangement (□: pilot; ∘: guard symbols; ×: data symbols)

(b) Rx symbol pattern (▽: data detection, ⊞: channel estimation)

Figure 5: OTFS symbol arrangement at transmitter and receiver[2]

The number of guard symbols that are placed depends on the maximum delay of the channel. Since the Doppler spread is not known, if it is not an integer multiple of the Doppler resolution, entire column is used as guard symbols. After estimating the channel matrix, equalisation is done in Delay-Doppler domain.
The received channel matrix is in the form,

$$H_{rec} = (pilot) * H2 + noise$$

where $H_{rec}$ = received channel matrix
$H2$ = true channel matrix
The channel matrix is estimated from the received channel matrix by zeroing the elements whose contribution is very small for output. Finding a threshold and zeroing the elements whose magnitude is smaller than threshold is a way to do it. Conventionally, Absolute thresholding is used.

**Absolute thresholding**

The noise is assumed to be complex Gaussian with standard deviation $\sigma$. The pilot scales the true channel and then it is corrupted by noise. The zero indices in the true channel matrix contain only noise. Based

on the property of a Gaussian distribution that majority of them lies within a threshold, a threshold is decided where all elements with magnitude less than the threshold are zeroed.
In absolute thresholding, the knowledge of the noise variance is needed. The absolute threshold depends on noise variance.

One contribution of this thesis is the determination of an adaptive threshold which is independent of the channel statistics and noise variance.

**Adaptive thresholding**

In adaptive thresholding, the threshold is decided based on the values of the received channel matrix. Since the channel matrix is a sparse matrix, most of the elements are zero. This fact can be used to find the threshold. In this work, two methods are proposed.

- **Knee point method:** The received channel matrix is sorted based on their magnitude. A monotonically decreasing graph can be observed. Knee point is the point where the magnitude of the values in the graph changes drastically after crossing the point. Knee points are found two times. After the first time, the elements in the channel matrix with very high magnitude are eliminated. The knee point found at the second time is used as the threshold.
- **One-sided trimmed mean method:** Since the channel is a sparse matrix, more than half of the channel matrix is zero. Majority of the received channel matrix will only contain noise. The mean of magnitude of the smaller fifty percent matrix is approximated to the mean of a Rayleigh random variable from which the noise variance can be estimated. The threshold is found based on this estimated noise variance.

## 2.4 Peak to Average Power Ratio

Peak to Average Power Ratio (PAPR) is one of the metric commonly used in context of communication in multicarrier systems. The data before transmitted goes through a power amplifier.
For power amplifier to work properly, the peak power of the transmitted data should be below the saturation limit. PAPR measures how much the peak of the data is away from mean of the data. PAPR should be low for power amplifier to work properly. For a system, if PAPR is high, the transmitted data should scaled down such that its peak is below the saturation limit.

## 2.5 Results and Discussion

The performance of pilot aided channel estimation for OTFS is studied for different pilot powers. The SNR of pilot, called $SNR_p$, is used as the basis for all comparisons. Bit error rate (BER) is the measure of performance. For coded BER, turbo encoding with 2/3 rate is used.

### 2.5.1 Performance of OTFS With Different $SNR_p$

The performance of pilot aided channel estimation of OTFS with different $SNR_p$ for an Extended Vehicular A (EVA) channel is studied for a maximum Doppler spread of 444Hz. Figure 6 shows the uncoded and coded BER of pilot aided OTFS with ideal channel estimate of OTFS for M = 256 and N = 8.

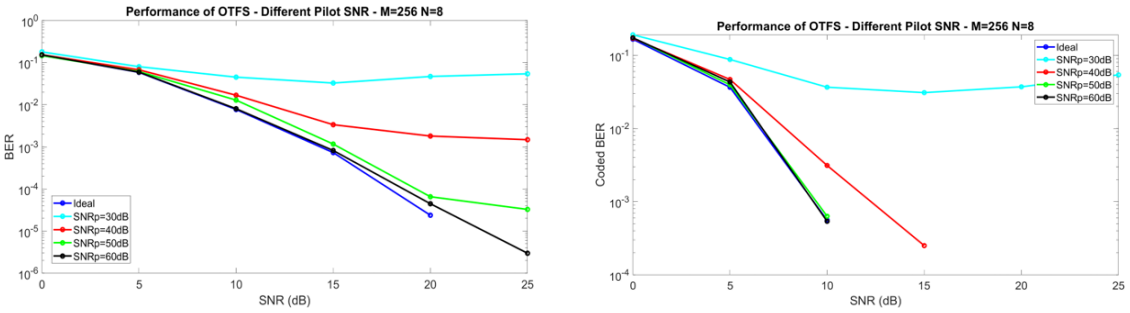


(a) Uncoded BER

(b) Coded BER

Figure 6: OTFS BER vs SNR for different $SNR_p$ for EVA channel M = 256 and N =8

As SNRp increases, the performance of OTFS approaches the ideal performance. After SNRp = 60dB, the performance of OTFS saturates to the ideal performance. For OTFS to have good performance its $SNR_p$ should be atleast 20dB higher than the SNR of data ($SNR_d$).

### 2.5.2 Performance of OTFS with Different M

Figure 7 shows the performance of pilot aided channel estimation of OTFS for different M (number of subcarriers) and same N = 8.

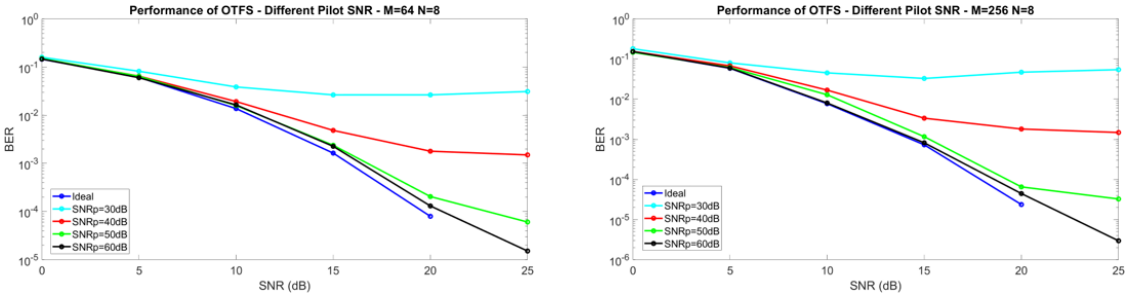


(a) Uncoded BER when M = 64




(b) Uncoded BER when M = 256

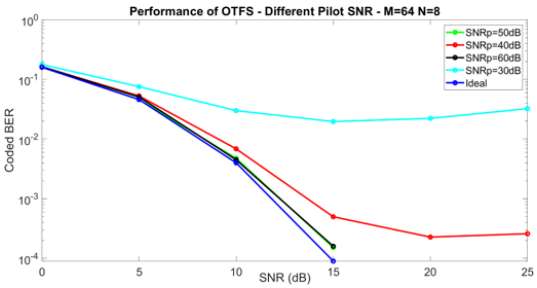


(c) Coded BER when M = 64

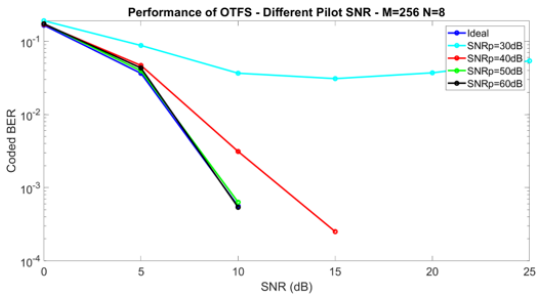


(d) Coded BER when M = 256

Figure 7: OTFS BER vs SNR for different M

As M increases, the resolution of the Delay-Doppler channel representation increases in delay dimension. This helps in better channel estimation which results in improvement of performance.

### 2.5.3 Performance of OTFS with Different N

Figure 8 shows the performance of pilot aided channel estimation of OTFS for different N and M = 64.

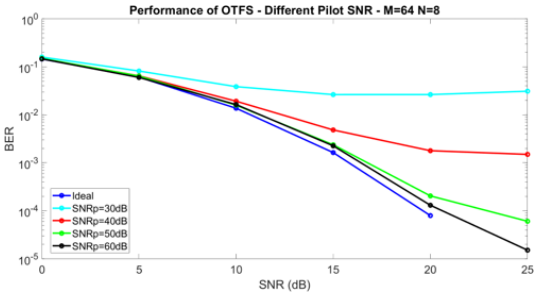


(a) Uncoded BER when N = 8

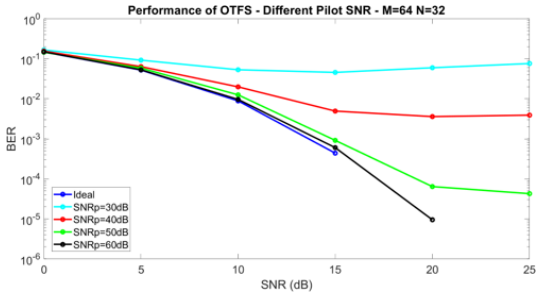


(b) Uncoded BER when N = 32

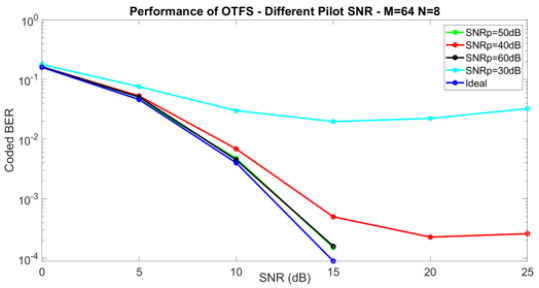


(c) Coded BER when N = 8

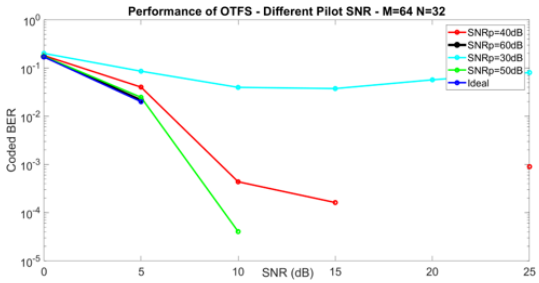


(d) Coded BER when N = 32

Figure 8: OTFS BER vs SNR for different N

As N increases, the resolution of the Delay-Doppler channel representation increases in Doppler dimension. This helps in better channel estimation which results in improvement of performance.

### 2.5.4 Importance of M and N in OTFS

Figure 9 shows the comparison of the performance of pilot aided channel estimation of OTFS for same M*N = 2048.

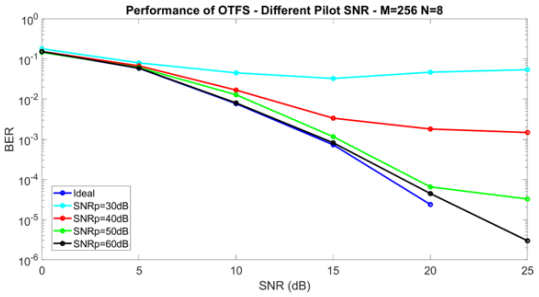


(a) Uncoded BER when N = 8 M = 256

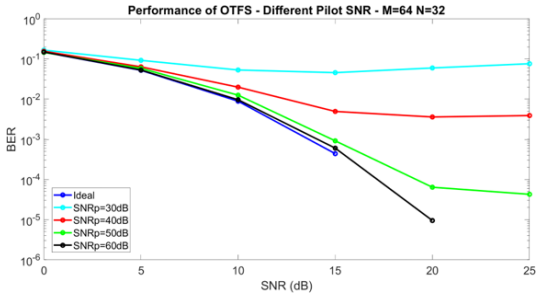


(b) Unoded BER when N = 32 M = 64

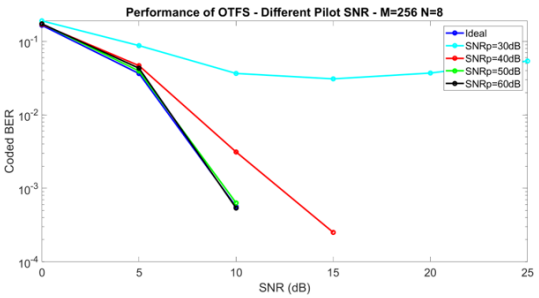


(c) Coded BER when N = 8 M = 256

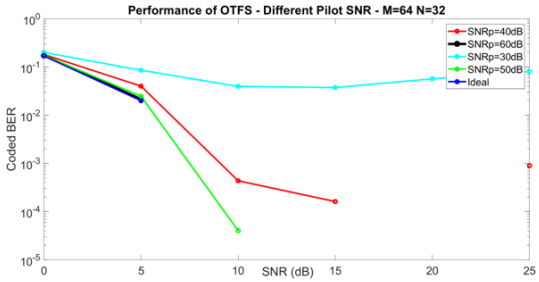


(d) Coded BER when N = 32 M = 64

Figure 9: OTFS BER vs SNR for same M*N value

The 64-32 curve falls faster than 256-8 curve. Accuracy of the channel gets better when M and N are as large as possible. For a constant M*N value, choosing larger M and N will give better performance for OTFS.

### 2.5.5 Performance of Adaptive Thresholding in OTFS Channel Estimation

Figure 10 shows comparison of performance of pilot aided channel estimation of OTFS with absolute thresholding and adaptive thresholding methods for different $SNR_p$ in an EVA channel with maximum Doppler of 444Hz. Here $4\sigma$ and $5\sigma$ are used as absolute thresholds and two knee point thresholds and trimmed mean threshold are used as adaptive thresholds.

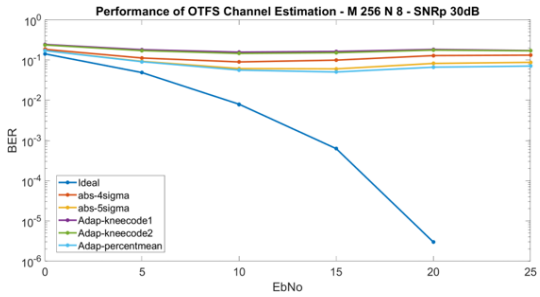


(a) Uncoded BER at $SNR_p = 30$dB

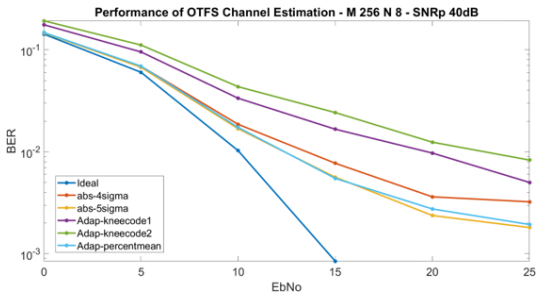


(b) Uncoded BER at $SNR_p = 40$dB

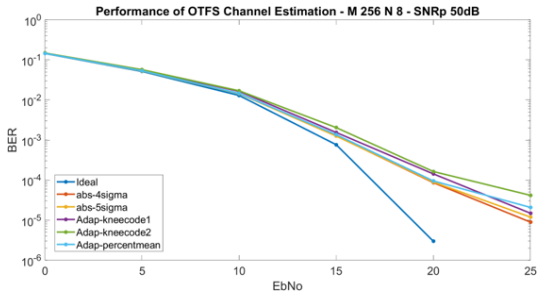


(c) Uncoded BER at $SNR_p = 50$dB

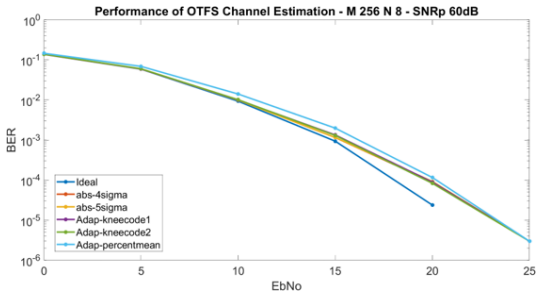


(d) Uncoded BER at $SNR_p = 60$dB

Figure 10: OTFS uncoded BER vs SNR with different thresholding methods for EVA channel

The adaptive threshold performance is closer to the absolute thresholding methods. They both approach ideal performance as $SNR_p$ increases. The rate of approach is much higher for coded BER. The adaptive thresholding and absolute thresholding performance are much closer.

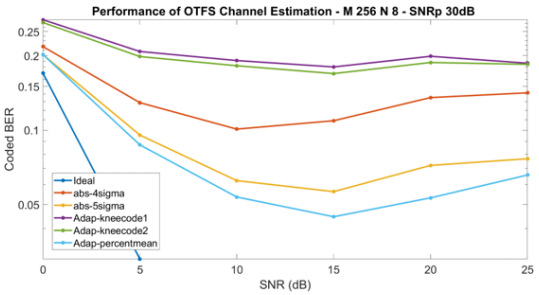


(a) Coded BER at $SNR_p = 30$dB

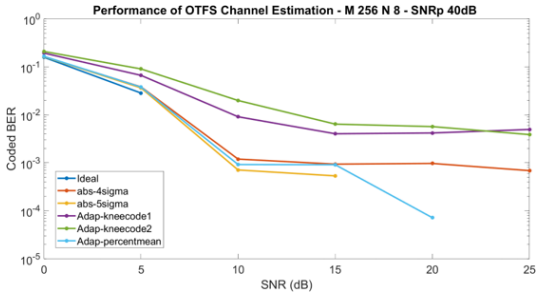


(b) Coded BER at $SNR_p = 40$dB

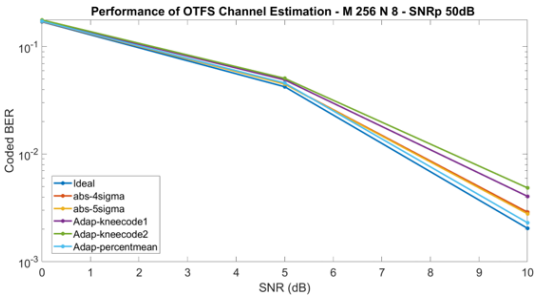


(c) Coded BER at $SNR_p = 50$dB

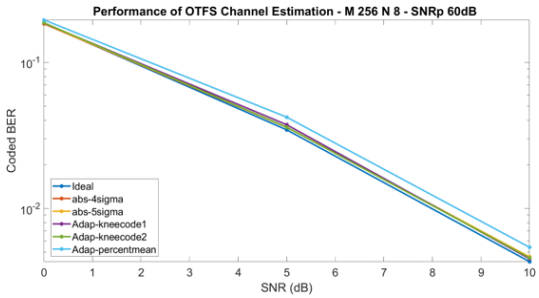


(d) Coded BER at $SNR_p = 60$dB

Figure 11: OTFS coded BER vs SNR with different thresholding methods for EVA channel

These methods gave consistent results when simulated with ETU channel with maximum Doppler = 444Hz. Figure 12 shows the performance of OTFS when adaptive thresholding methods are used.

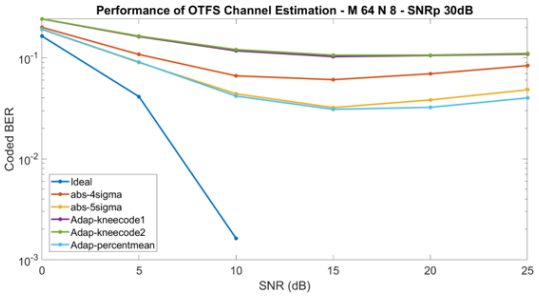


(a) Coded BER at $SNR_p = 30$dB

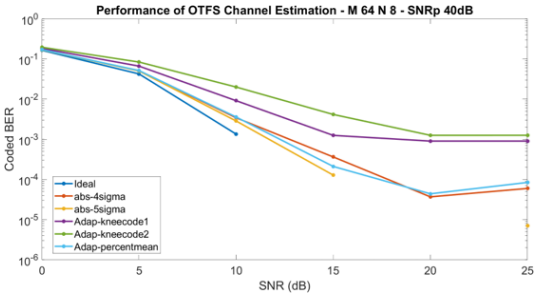


(b) Coded BER at $SNR_p = 40$dB

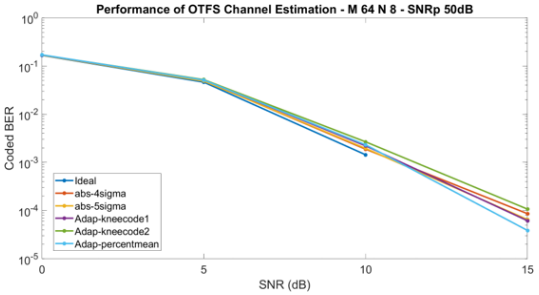


(c) Coded BER at $SNR_p = 50$dB

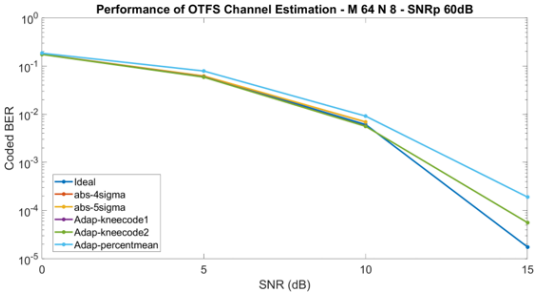


(d) Coded BER at $SNR_p = 60$dB

Figure 12: OTFS Coded BER vs SNR with different thresholding methods for ETU channel

### 2.5.6 Comparison of OTFS with MC-CDMA Schemes With Known Channel

Figure 13 shows the performance of OTFS and MC-CDMA schemes for a known channel. The channel used for comparison is EVA channel with a maximum doppler spread of 444Hz.

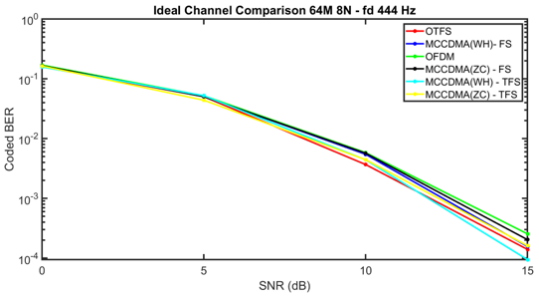


(a) Coded BER for M=64 N = 8

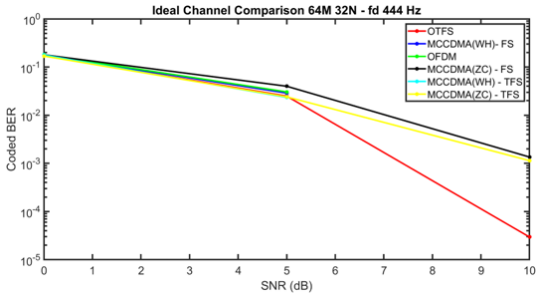


(b) Coded BER for M=64 N = 32

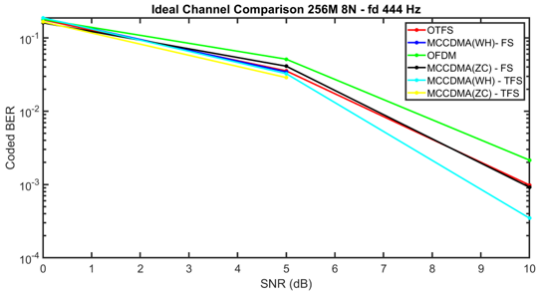


(c) Coded BER for M=256 N = 8

Figure 13: Coded BER vs SNR comparison of OTFS and MC-CMDA for a known channel for different N and M

The known channel performance of OTFS and MC-CDMA are similar. OTFS and MC-CDMA have better performance compared to OFDM because of transmit diversity.

For fair comparison between performance of OTFS and MC-CDMA, same amount of overhead, same total transmit power and same average transmit power per symbol are maintained. To maintain this condition, different types of power allocations for pilots and data are implemented in MC-CDMA. They are:

- **Pilots-only Boosting** Only pilots are boosted (the energy of one pilot in OTFS is distributed over entire overhead symbols). Thus total transmit power will be same as OTFS.
- **Grid Boosting** Both pilots and data symbols used are of same

energy. Based on the total overhead of OTFS (one pilot and some guards), the entire resource grid is boosted to match the total transmit power of OTFS.

- **Differential Boosting** The pilots and data symbols are boosted differently based on a ratio to match the total transmit power of OTFS.

Differential Boosting is generic situation. Both Grid Boosting and Pilot Boosting can be considered as a type of Differential Boosting. For same noise scenario, Grid Boosting will have higher SNR compared to Pilot Boosting as data symbols are boosted.

### 2.5.7 Comparison of PAPR of OTFS and MC-CDMA Schemes for Different $SNR_p$

Figure 14 shows PAPR of different schemes at $E_b/N_0 = 10$dB for different $SNR_p$ at M = 64 and N = 8 in EVA channel with a maximum Doppler of 444Hz.

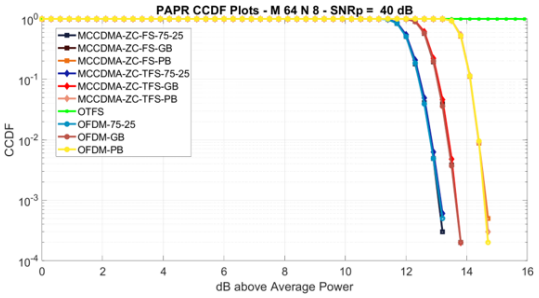


(a) PAPR when $SNR_p$ = 40dB

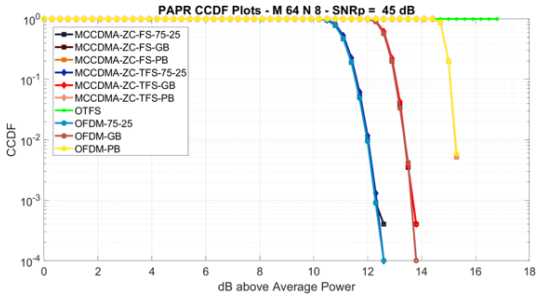


(b) PAPR when $SNR_p$ = 45dB

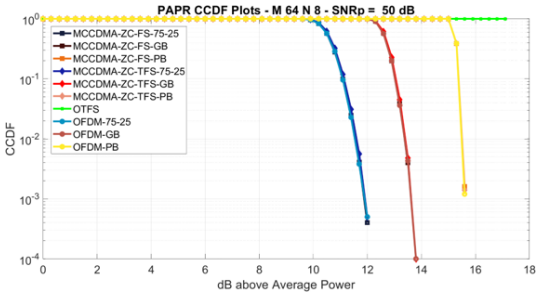


(c) PAPR when $SNR_p$ = 50dB

Figure 14: PAPR of all schemes at different $SNR_p$ for M= 64 and N = 8

The PAPR depends on the $E_b/N_0$ values as pilot power in OTFS is different for different $E_b/N_0$. PAPR of OTFS increases as $SNR_p$ increases but for higher $E_b/N_0$ the rate of increase of PAPR decreases. PAPR of OTFS and Pilot Boosting schemes decreases as $E_b/N_0$ increases. The PAPR of Grid Boosting remains constant, as the entire grid is boosted.

Figure 15 shows PAPR of different schemes at $E_b/N_0$ = 10dB for different $SNR_p$ at M = 256 and N = 8 in EVA channel with a maximum Doppler of 444Hz.

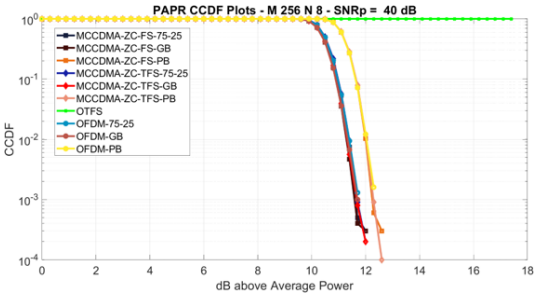


(a) PAPR when $SNR_p = 40$dB

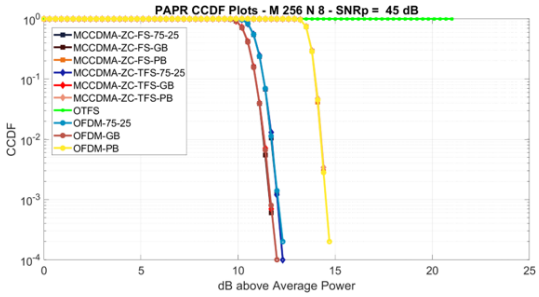


(b) PAPR when $SNR_p = 45$dB

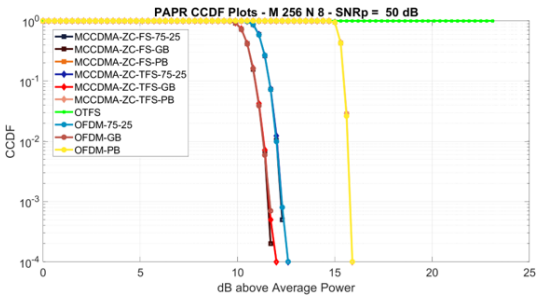


(c) PAPR when $SNR_p = 50$dB

Figure 15: PAPR of all schemes at different $SNR_p$ for M = 256 and N = 8

For same N, PAPR of OTFS and Pilot boosting increases with increase in M. PAPR of 75-25 scheme increases as $E_b/N_0$ increases.
Figure 16 shows PAPR of different schemes at $E_b/N_0 = 10$dB for different $SNR_p$ at M = 64 and N = 32 in EVA channel with a maximum Doppler of 444Hz.

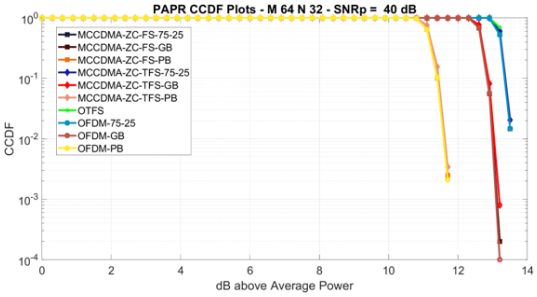


(a) PAPR when $SNR_p$ = 40dB

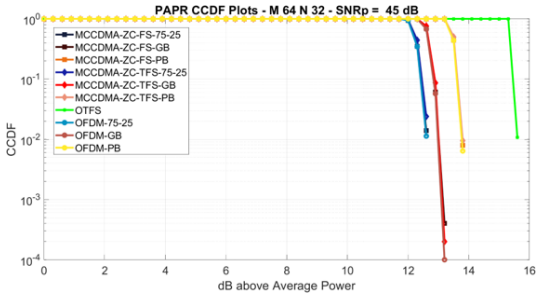


(b) PAPR when $SNR_p$ = 45dB

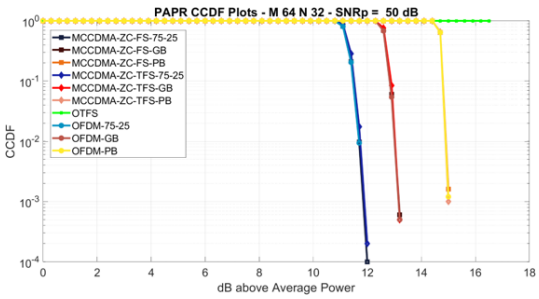


(c) PAPR when $SNR_p$ = 50dB

Figure 16: PAPR of all schemes at different $SNR_p$ for M = 64 and N = 32

For same M, PAPR of OTFS decreases as N increases. PAPR of OTFS and pilot boosting decreases as $E_b/N_0$ increases. In all the above situations, PAPR of MC-CDMA and OFDM remains same for Grid Boosting.

### 2.5.8 Comparison of OTFS With MC-CDMA Schemes With Pilot Aided Channel Estimation

Performance of OTFS with pilot aided channel estimation is compared with MC-CDMA by three different pilot arrangements ,i.e Grid Boosting, Pilot Boosting and Differential Boosting. In differential boosting data and pilots are boosted in 3:1 ratio. All these schemes are compared for same noise scenario.

Figure 17 shows the comparison of OTFS and MC-CDMA with grid

boosting for different $SNR_p$ at M = 64 and N = 8 for EVA channel with a maximum Doppler spread = 444Hz.

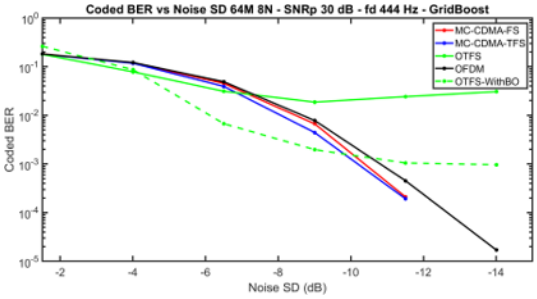


(a) Coded BER when $SNR_p$ = 30dB

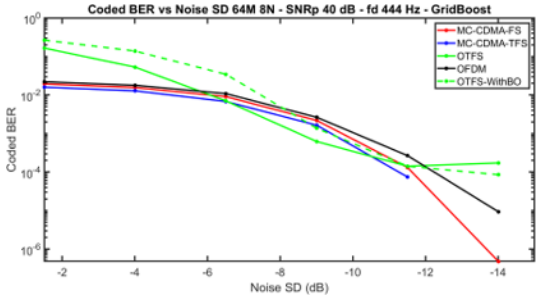


(b) Coded BER when $SNR_p$ = 40dB

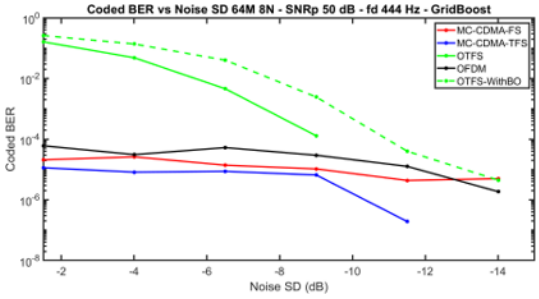


(c) Coded BER when $SNR_p$ = 50dB

Figure 17: Coded BER vs noise standard deviation for all schemes at different $SNR_p$ with grid-boosting for M = 64 and N = 8 for EVA channel with maximum Doppler = 444Hz

The MC-CDMA-TFS schemes with grid boosting always outperform OTFS at higher noise scenarios as both schemes have different SNR. As $SNR_p$ increases, OTFS performance will become comparable to MC-CDMA -TFS. Only for $SNR_p$ = 30dB, the PAPR of OTFS is less than that of MC-CDMA. So, because of Back off it's SNR improved which resulted in better performance when compared to the one without Back Off.

Figure 18 shows the comparison of OTFS and MC-CDMA with grid boosting for different $SNR_p$ at M = 64 and N = 8 for EVA channel with a maximum Doppler spread = 1000Hz.

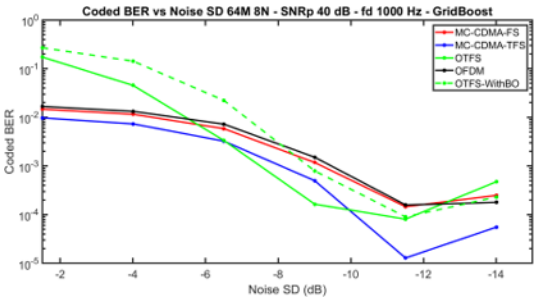


(a) Coded BER when $SNR_p$ = 30dB

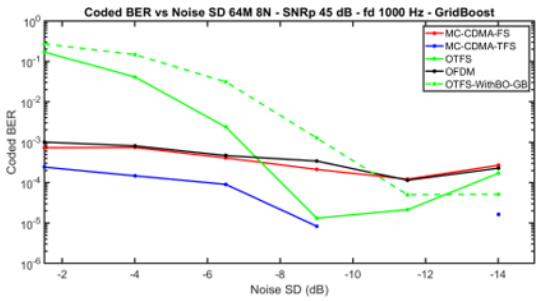


(b) Coded BER when $SNR_p$ = 40dB

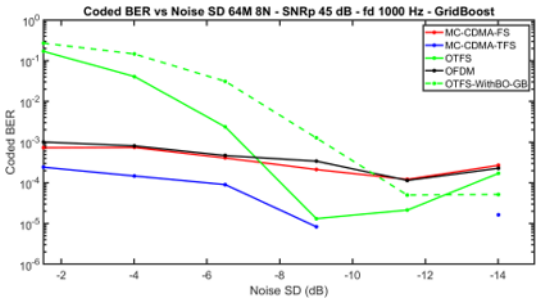


(c) Coded BER when $SNR_p$ = 50dB

Figure 18: Coded BER vs noise standard deviation for all schemes at different $SNR_p$ with grid-boosting for M = 64 and N = 8 for EVA channel with maximum Doppler = 1000Hz

Performance of OTFS improves as $SNR_p$ increases without Back Off, where as it decreases as $SNR_p$ increases with Back Off.

Figure 19 shows the comparison of OTFS and MC-CDMA with differential boosting with ratio 3:1 for different $SNR_p$ at M = 64 and N = 8 for EVA channel with a maximum Doppler spread = 444Hz.

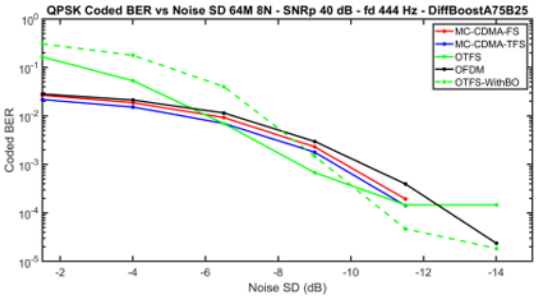


(a) Coded BER when $SNR_p = 40$dB

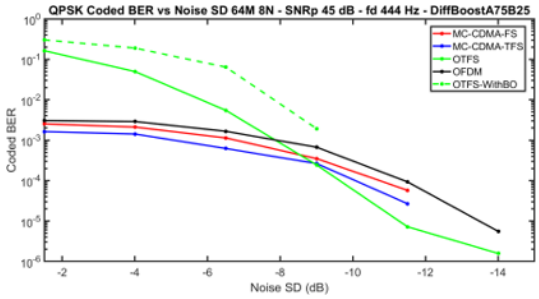


(b) Coded BER when $SNR_p = 45$dB

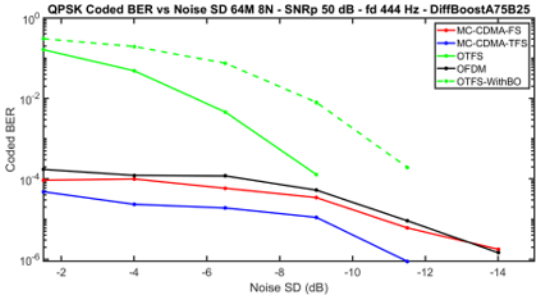


(c) Coded BER when $SNR_p = 50$dB

Figure 19: Coded BER vs noise standard deviation for all schemes at different $SNR_p$ with differential boosting for M = 64 and N = 8 for maximum Doppler = 444Hz

Performance of OTFS improves as $SNR_p$ increases without Back Off, where as it decreases as as $SNR_p$ increases with Back Off. MC-CDMA with Differential Boosting outperforms OTFS as the ratio at which data and pilot are boosted increases the SNR. At lower nosie levels, OTFS becomes better than MC-CDMA because of its low PAPR.

Figure 20 shows the comparison of OTFS and MC-CDMA with pilot boosting for different $SNR_p$ at M = 64 and N = 8 for EVA channel with a maximum Doppler spread = 444Hz.

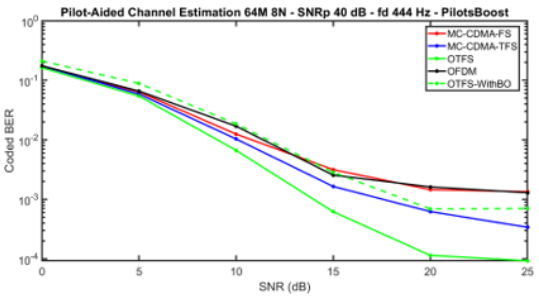


(a) Coded BER when $SNR_p = 40$dB

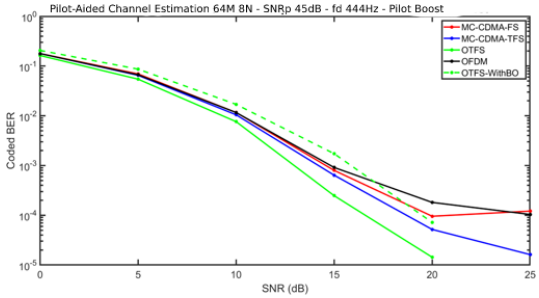


(b) Coded BER when $SNR_p = 45$dB

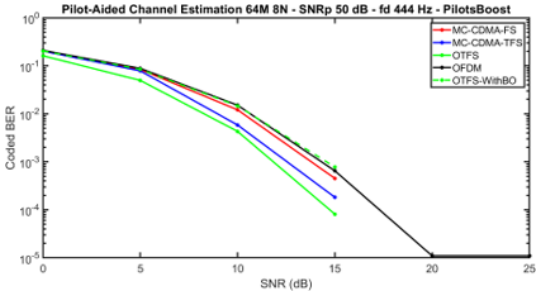


(c) Coded BER when $SNR_p = 50$dB

Figure 20: Coded BER vs SNR for all schemes with pilot boosting at different $SNR_p$ for M = 64 and N = 8 for maximum Doppler = 444Hz

OTFS without Back Off outperforms all other schemes. As $SNR_p$ increases, performance of OTFS with Back Off degrades.

Figure 21 shows the comparison of OTFS and MC-CDMA with pilot boosting for different $SNR_p$ at M = 64 and N = 8 for EVA channel with a maximum Doppler spread = 1000Hz.

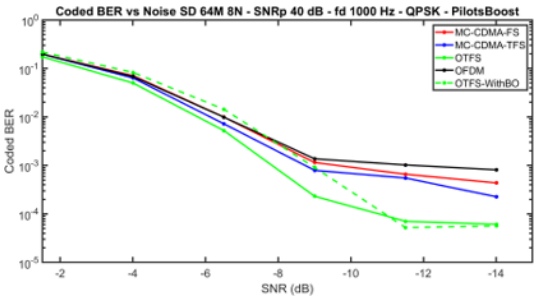


(a) Coded BER when $SNR_p = 40$dB

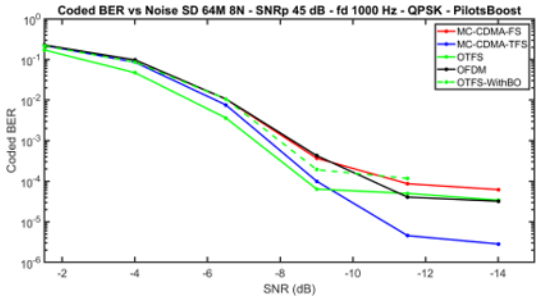


(b) Coded BER when $SNR_p = 45$dB

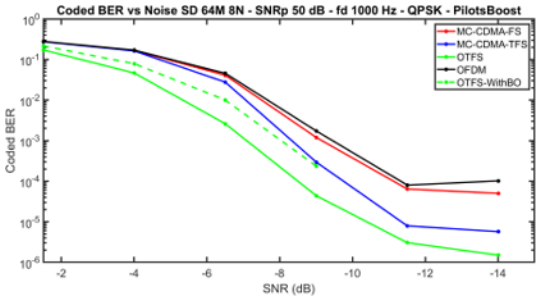


(c) Coded BER when $SNR_p = 50$dB

Figure 21: Coded BER vs noise standard deviation with pilot boosting for all schemes at different $SNR_p$ for M = 64 and N = 8 for maximum Doppler = 1000Hz

OTFS with Back Off at lower Doppler spread, for lesser $SNR_p$, is comparable to pilot boosted MC-CDMA schemes. For higher $SNR_p$, MC-CDMA with pilot boosting outperforms OTFS.

## 2.6 Conclusion

Thus the pilot aided channel estimation of OTFS modulation scheme is analyzed and is compared with various MC-CDMA schemes capturing the effect of PAPR also. A novel adaptive thresholding is also implemented for OTFS which is independent of the channel statistics and noise variance.

# TARGET CLASSIFICATION IN A DISTRIBUTED RADAR SYSTEM

## 3.1 Introduction

### 3.1.1 Motivation

Detecting type of target is a task with great importance because of its applications in military and surveillance fields. Target type can be classified if target shape or anything related to target shape and size are calculated. While doing target localization using multistatic radar, target position can be estimated and can also be tracked. Target positions can be calculated from the bistatic equations that are obtained. At the receiver the delay at which peak occurs after correlation with transmit signals is used to obtain the bistatic equations. The value at the peak of the correlation helps to determine the Radar Cross Section (RCS) value of the target.

The aim of this thesis is to calculate the Bistatic RCS of a target and classify whether it is a Fixed Wing Drone (FWD) or a Quadcopter Drone (QCD) based on the Bistatic RCS values at the receiver.

### 3.1.2 Scenario Considered

We have considered the scenario where targets are present in a 7 cell region with hexagon-hexagon distance of 3km. Each hexagonal cell consists of four towers which will be transmitting and receiving at different instants of time. At any given instant of time, one tower from a cell will be transmitter and the other 3 towers will be receivers.

Hence, we will have 7 transmitters and 21 receivers in the 7 cell region at every instant. For each set of 7 cells, there is a fusion centre which works independently and records all the Time of arrival (ToA)

values, the correlation peaks and bistatic Doppler frequencies corresponding to the all the transmitter-receiver pairs of the 7 cells. For every 6msec, the fusion centre would record a new set of ToA values (also called lags) corresponding to a snapshot of the targets. We make use of these lag values to find the position of the target. Then, using the correlation peaks corresponding to different transmitters at every receiver, Bistatic RCS values are calculated. Using these Bistatic RCS values, we try to classify the targets.

## 3.2 Background Information

### 3.2.1 Radar Cross Section

RCS is a measure of how detectable an object is by the radar. It is the fictional area representing that amount of power which, when scattered equally in all directions, produces an echo at the radar equal to that from the target.

$$\sigma = \lim_{R \to \infty} 4\pi R^2 (\frac{P_{Dr}}{P_{Di}})$$

$P_{Di}$= Power density of a wave incident on a target at range R away from RADAR
$P_{Dr}$ =Power density of scattered waves at the receiving antenna
RCS is measured in square meters (**m2**). It is often represented in logarithmic scale because of its large dynamic range with reference $\sigma_{ref} = 1m^2$.

$$\sigma_{dBsm} = \sigma_{dBm^2} = 10 \log_{10} \frac{\sigma_{m^2}}{\sigma_{ref}} = 10 \log_{10} \frac{m^2}{1} \tag{1}$$

### 3.2.2 Types of Radar Cross Section

There are two types of Radar Cross Section. They are Monostatic Radar Cross Section and Bistatic Radar Cross Section.

**Monostatic Radar Cross Section**

It is the RCS value observed by the transmitter that sent the EM wave or by a receiver at the same position as of the transmitter after hitting the target.

The monostatic radar equation is

$$P_r = \frac{P_t G^2 \lambda^2 \sigma}{(4\pi)^3 R^4} \tag{2}$$

Where

$\sigma$ = Monostatic Radar Cross Section

$P_t$ = Transmit power

$P_r$ = Received power

$G$ = Antenna gain

$\lambda$ = Wavelength of the signal

$R$ = Distance between the transmitter and the target

**Bistatic Radar Cross Section**

It is the RCS value observed by the receiver which is at a different place from the transmitter after hitting the target.

The bistatic radar equation is

$$P_r = \frac{P_t G_t G_r^2 \sigma_B}{(4)^3 R_t^2 R_r^2} \tag{3}$$

Where

$\sigma_B$ = Bistatic Radar Cross Section

$P_t$ = Transmit Power

$P_r$ = received power

$G_t, G_r$ = Antenna gain of transmitter and receiver respectively

$\lambda$ = Wavelength of signal

$R_t, R_r$ = Distance between the target with transmitter and receiver respectively

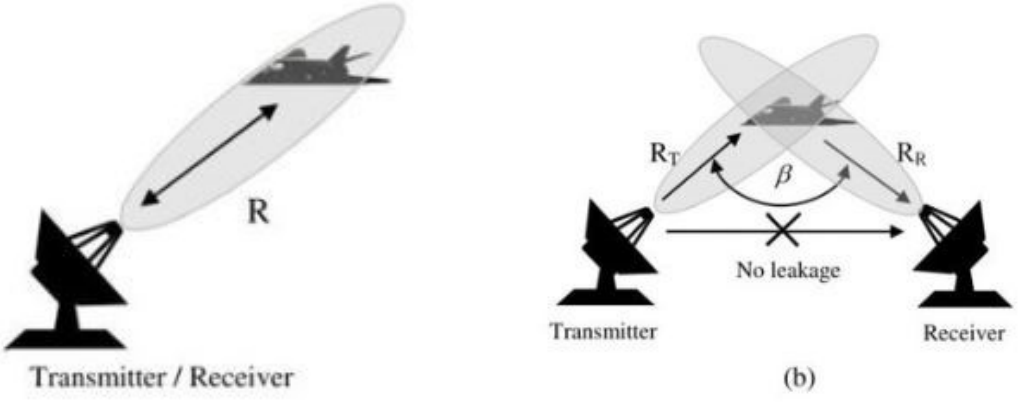


(a) Monostatic RCS

(b) Bistatic RCS

Figure 22: Types of RCS[3]

### 3.2.3 RCS Dependencies

RCS depends on factors like Target Geometry, Frequency, Angular orientation with respect to Transmitter and Receiver and Polarisation.

**Target Geometry and Frequency**
RCS of a target for a same frequency behaves differently for objects of different sizes. Based on the ratio of $\lambda$ and characteristic length, RCS can be categorised into different regions. They are Rayleigh region, Mie resonance region and Optical region. Figure 2 is an example of how RCS varies for a metallic sphere of size a.

**Angular Orientation**
RCS values depends on the orientation of the target with respect to transmitter and receiver. Whenever there is some kind of peak in the surface of the target, it's RCS values will have a peak.

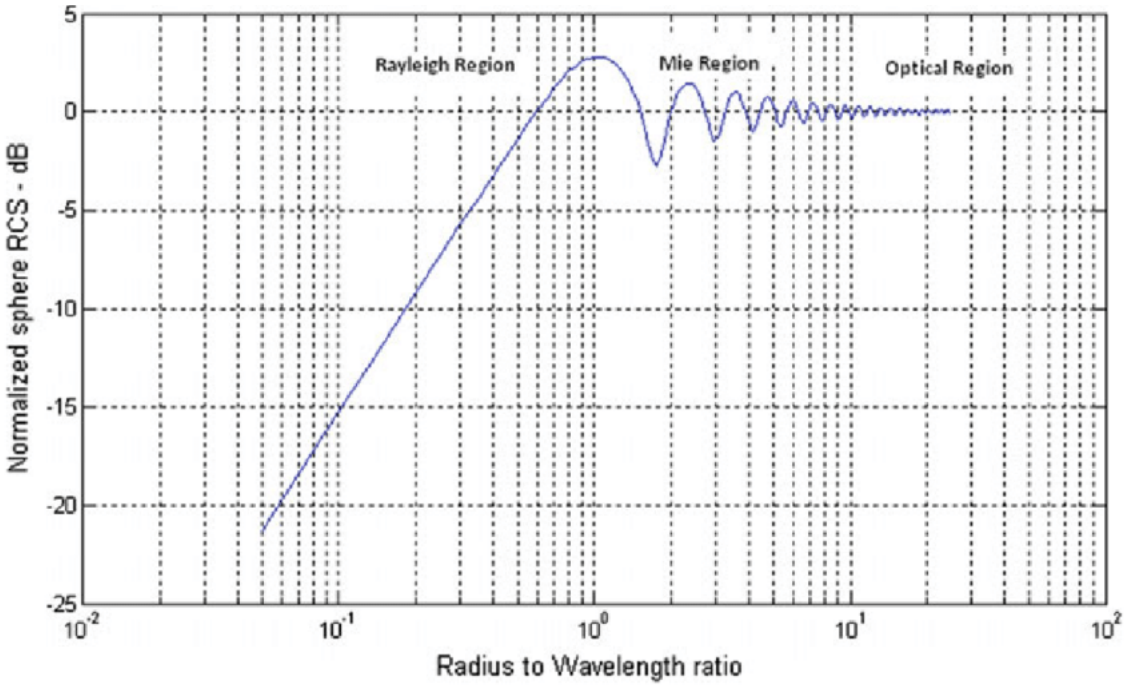


Figure 23: RCS for different object size[4]

**Polarisation**

When an electromagnetic wave hits the target, the wave will be scattered off the target and some energy will be transferred between two orthogonal polarization components. Hence, target scattering mechanism is often modeled by a 2x2 Radar Cross Section (RCS) matrix (scattering matrix), whose diagonal terms specify how the target scatters the energy into the original H and V polarization component and off diagonal terms specify how the target scatters the energy into the opposite polarization component.

Because the transmit and receive antennas can have any combination of polarizations, it is often of interest to look at the polarization signature for a target for different polarization configurations as a function of the tilt angle and the ellipticity angle of the transmit polarization ellipse. This can also be seen as a measure of the effective RCS.

Two most widely used polarization signatures (also known as polariza-

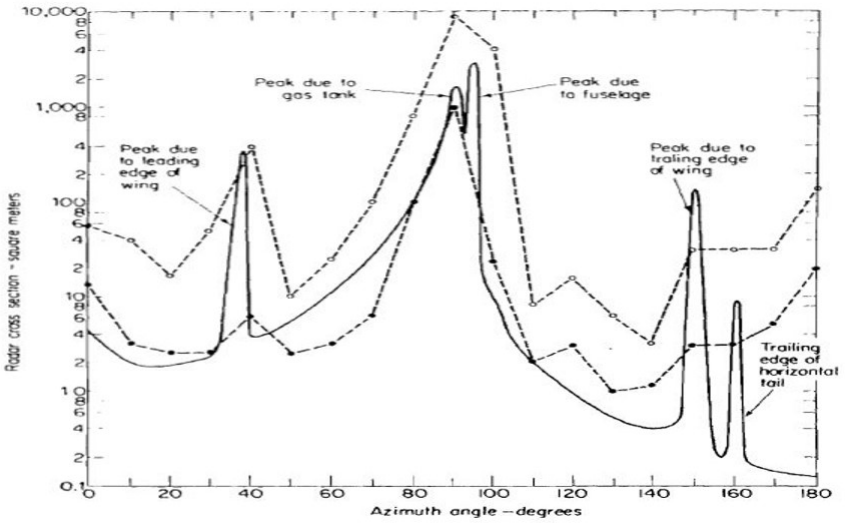


Figure 24: Comparison of theoretical and model measurements RCS of a B-47 medium bomber jet aircraft at a frequency of 980 MHz (solid line)/600 MHz (dashed curve)

tion responses), are co-polarization (response uses the same polarization for both transmit and receive) response and cross polarization (uses the orthogonal polarization in receive) response.

## 3.3 Bistatic RCS Recovery

Bistatic RCS has some information about the target shape and size. It can be estimated from the Bistatic Radar Equation.

$$P_r = \frac{P_t G_t G_r \lambda^2 \sigma_B}{(4\pi)^3 R_t^2 R_r^2} \tag{4}$$

In the scenario considered, transmit power of the incident wave is known. The antenna patterns of the transmitter and receiver are known. Wavelength of the incident wave is known.

In multi-static simulator, at the receiver, the received signal is correlated with the local copy of the transmitted waveforms which are known. The peak of the correlator output is the received power. Thus,

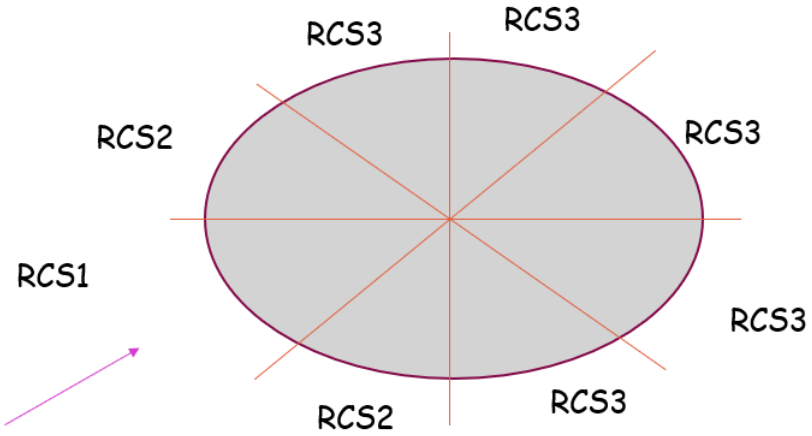


Figure 25: The dummy target model

the received power is also known. The lags of peaks of the correlator outputs are used to estimate the target location.

All the remaining parameters in bistatic radar equation can be calculated if the target location is known. After, estimated position of target is calculated, Bistatic RCS values are recovered.

### 3.3.1 Experiment with Dummy Target

To verify whether the estimated Bistatic RCS values are same as the true Bistatic RCS values, a dummy target is considered. The dummy target has the following property. The Bistatic RCS of the target are discrete. They depend on the bistatic angle between the target, Tx and Rx.
The target has 3 discrete Bistatic RCS values. If the bistatic angle is less than 450, it experiences 1.5 $m^2$ of RCS. If the angle is between 450 and 900, it experiences 7.5 $m^2$ of RCS else Bistatic RCS is 0.3 $m^2$ .

### 3.3.2 Observations

Most of the estimated RCS values are centered around the true RCS values. There are considerable amount of estimated RCS with value zero. These are because at the receiver, the peak of the correlation banks did not exceed the threshold. There are also few values that strayed far too much compared to the true values. To correctly identify the target, we need correct RCS values.

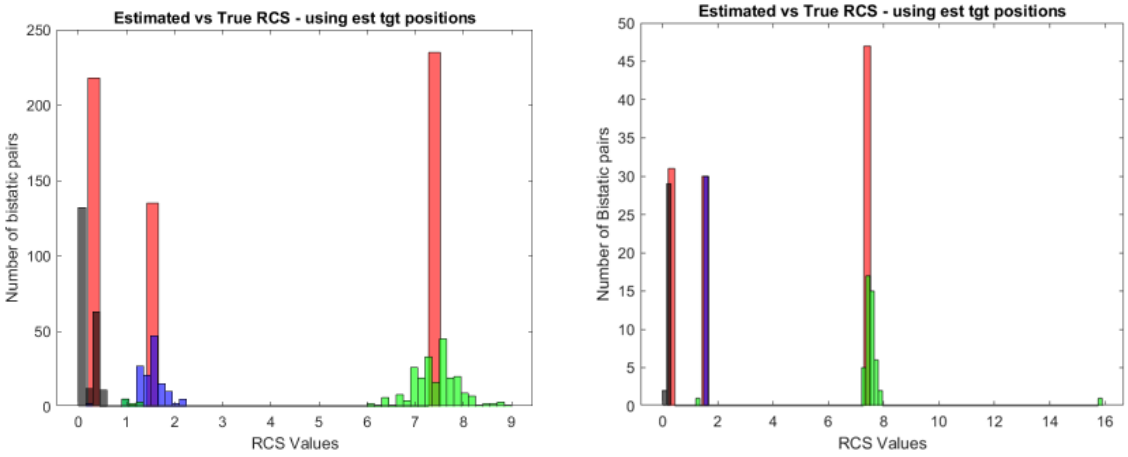


(a) with 7 Tx and 21 Rx

(b) with 1Tx and 27Rx

Figure 26: Ratio of Estimated RCS to True RCS

The estimated values that deviated too far from the true RCS are the ones from the Tx-Rx pairs which are directly below the target. If any tower is directly below the target, because of the error in target position calculation, the antenna gains calculated will deviate too much from the true antenna gains. To avoid these values, these rcs values are not considered for future target classification scenarios. The rcs values from such towers are directly zeroed. These are the estimated RCS values after this modification. Figure 26 shows the histogram of ratio of the estimated RCS to true RCS for different number of transmitters and receivers. The bar at 0 indicates only those number of bistatic pairs for which RCS went undetected.

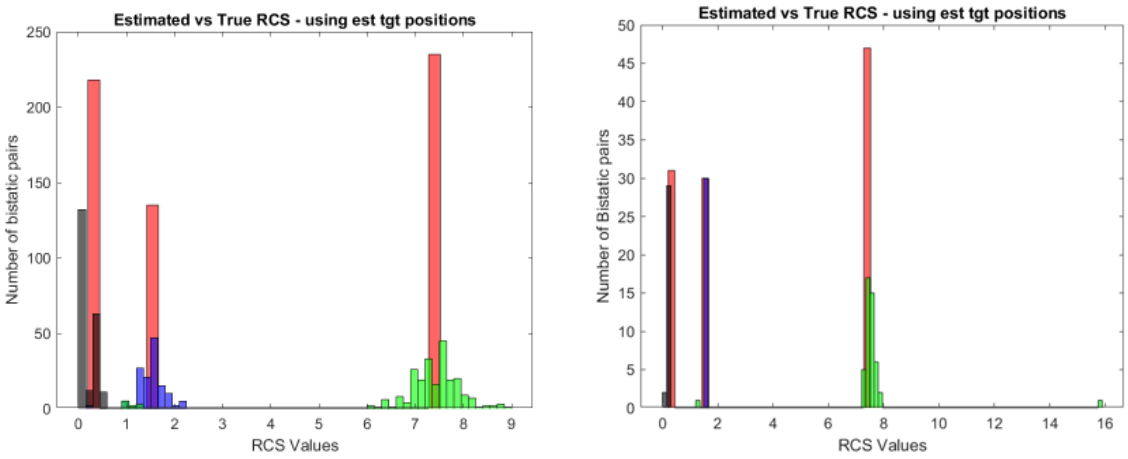


(a) with 7 Tx and 21 Rx

(b) with 1Tx and 27Rx

Figure 27: Ratio of Estimated RCS to True RCS after removing Tx-Rx pairs directly below target

Figure 27 shows the histogram of ratio of the estimated RCS to true RCS for different number of transmitters and receivers. The bar at 0 indicates those number of bistatic pairs for which RCS went undetected and those that are directly below the target.

## 3.4 Target Modelling

In this thesis, quadcopters and fixed wing drones are the only targets that are considered. Based on the RCS values the target should be identified. There is no direct method way of expressing RCS of such complex targets as there are no theoretical models for these drones. The Bistatic RCS of a quadcopter and fixed wing drone are simulated using software called Ansys HFSS. These values are hardcoded as models for target for simulation. 2 quadcopters and 2 fixed wing drones were considered.

### 3.4.1 Simulation of Bistatic RCS in HFSS

- Load the CAD model of the drone taken from GrabCAD library for which the RCS values are going to be calculated. Assign material type to the parts of the drone. The body of the drone is made of polystyrene. Batteries and motors are made of aluminium. The wiring is made of copper.
- Create an airbox around the drone. The dimensions for the airbox should be such that each edge is atleast $\lambda/4$ away from the drone.
- Create PML boundaries for the airbox with minimum frequency 500MHz. Use default settings for PML boundaries.
- Create length-based mesh for the airbox.
- Set excitation wave as plane wave in spherical co-ordinates. Specify all the incident directions for which RCS values should be calculated.
- In the Analysis window, select 500MHz as frequency at which HFSS will solve RCS values.
- After Validation check, Analyze All command solves the Maxwells equations to get RCS values.
- After simulation is completed, to obtain Bistatic RCS, an infinite sphere is to be setup with the angles where we are going to observe RCS values.
- The Bistatic RCS values can be observed in the Results section. To obtain the Bistatic RCS plot, in the Results section click on the far field report. The solved values can also be exported to a CSV file.

### 3.4.2 RCS of the Simulated Drones

The following are the observed RCS patterns of the simulated drones. There are 2 quadcopters and 2 Fixed wing Drones. In this project, the

drones are assumed to be staying in same horizontal plane. The drone blades are assumed to be static. In the following plots, the RCS patterns of target at incident elevation 1300 and reflection elevation angle 1300 for different incident azimuth angles are shown.

**RCS Pattern of Quadcopter**

The Quadcopter has a four-fold symmetry. So the same RCS pattern will be observed atmost 8 times for a given incident and reflection azimuth angles. Figure **??** and Figure 28 shows the RCS pattern of a quadcopter at the incident azimuth angles $50^0, 40^0, 310^0, 320^0, 140^0, 130^0, 220^0, 230^0$ degrees are shown. Based on the symmetry all these will have similar pattern.

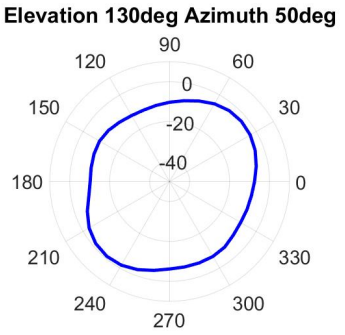


(a)

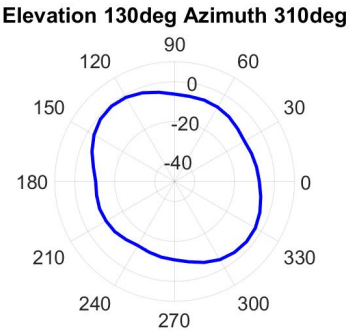


(b)

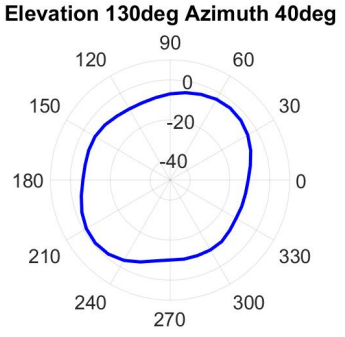


(c)

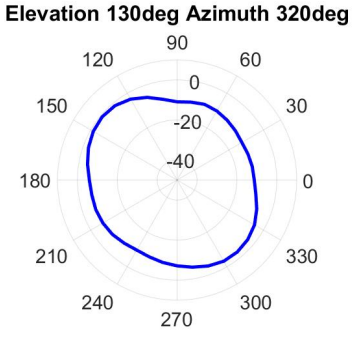


(d)

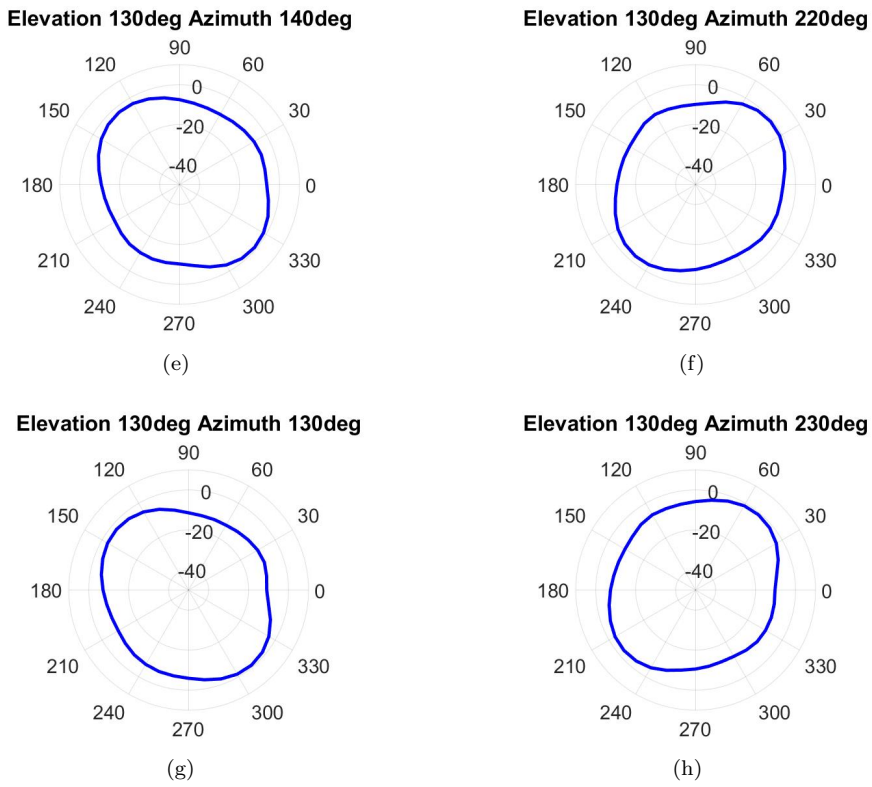


(e) (f) (g) (h)

Figure 28: RCS of a quadcopter on 8 symmetric angles

## RCS Pattern of Fixed Wing Drone

The Fixed Wing Drone has a two-fold symmetry. So the same RCS pattern will be observed atmost 2 times for a given incident and reflection azimuth angles. Figure 29 shows the RCS pattern of a fixed wing drone at the incident azimuth angles pairs $(50^0, 310^0)$, $(40^0, 320^0)$, $(140^0, 220^0)$, $(130^0, 230^0)$ degrees are shown. Based on the symmetry all these will have similar pattern.

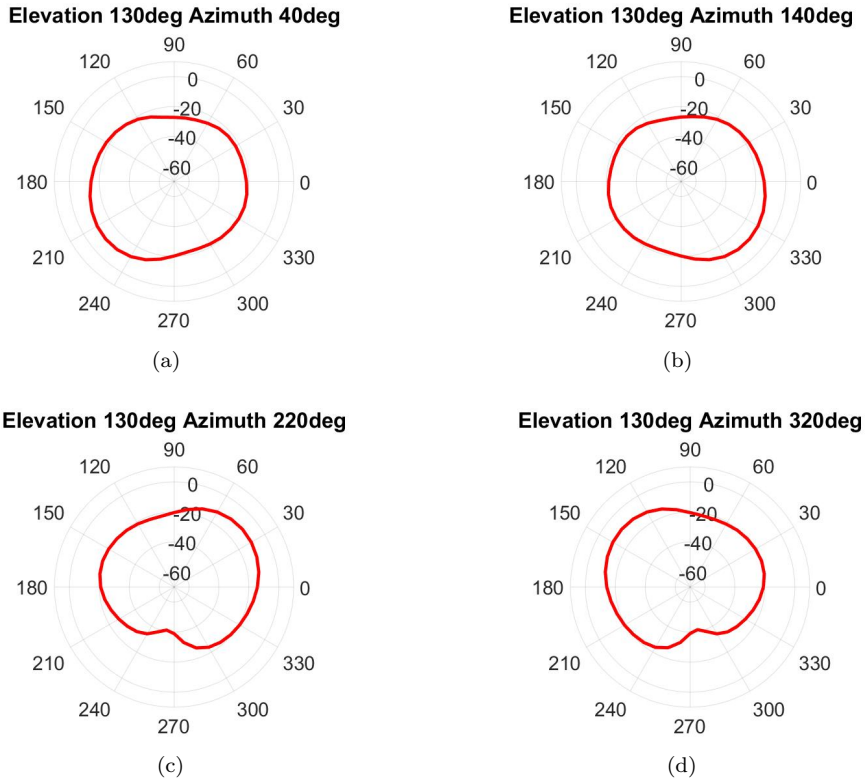


Figure 29: RCS of a fixed wing drone on pairs of symmetric angles

## 3.5 Target Classification

Two metrics are proposed for classification of the target based on the RCS values estimated at the receiver. They are Similarity metric and Symmetric metric.

### 3.5.1 Similarity Metric

In this method, The Quadcopters and Fixed wing drones are assumed to be clustered in two groups in a higher dimensional space. So to classify the target, the normalized version of the received RCS is taken, and its distance with the true RCS of the centroid of each class is taken. The target is classified into the class with minimum distance to the cluster.

$Error(e) = e_1 + e_2 + \ldots + e_{N_{hops}}$ where $e_l = \|estrcs - truercs_k\|_p$, p=1,2 k=cluster number.

### 3.5.2 Symmetric Metric

In this method, the received RCS values at the elevation angles equal to the mode of incident elevation angles are taken. The incident azimuth angles are divided into 12 parts and RCS values for these incident azimuth angles are considered. Since both the quadcopter and fixed wing drone has different types of symmetry, the RCS values at symmetric incident azimuth positions should be correspondingly equal. This symmetry of the targets is exploited.

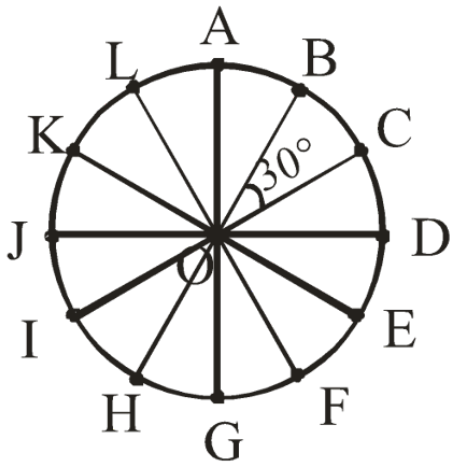


Figure 30: Approximated incident azimuth angles

Two errors are calculated. One error is from (B,C), (L,K), (I,H), (E,F) pairs of incident angles (QER), where as another is from (C,E), (B,F), (L,H), (K,I) pairs of incident azimuth angles (FER). If the target drone is a Quadcopter both errors will be similar to each other. If it is a Fixed Wing Drone, first error will be greater than the second error.

## 3.6 Results and Discussions

These are the following results and observations.

### 3.6.1 Accuracy of Estimated RCS

Figure 31 shows the histogram of the ratio of estimated to true RCS values for the two quadcopters and fixed-wing drones. Bar 0 indicates those bistatic RCS pairs that went undetected and those canceled because of a larger error in estimation as the tower is present exactly below the target. The ratio is mostly centered around 1 with a small variation which indicates the accuracy of the estimated RCS values by the algorithm. The total number of bistatic RCS values varies for each drone as their RCS values are different.

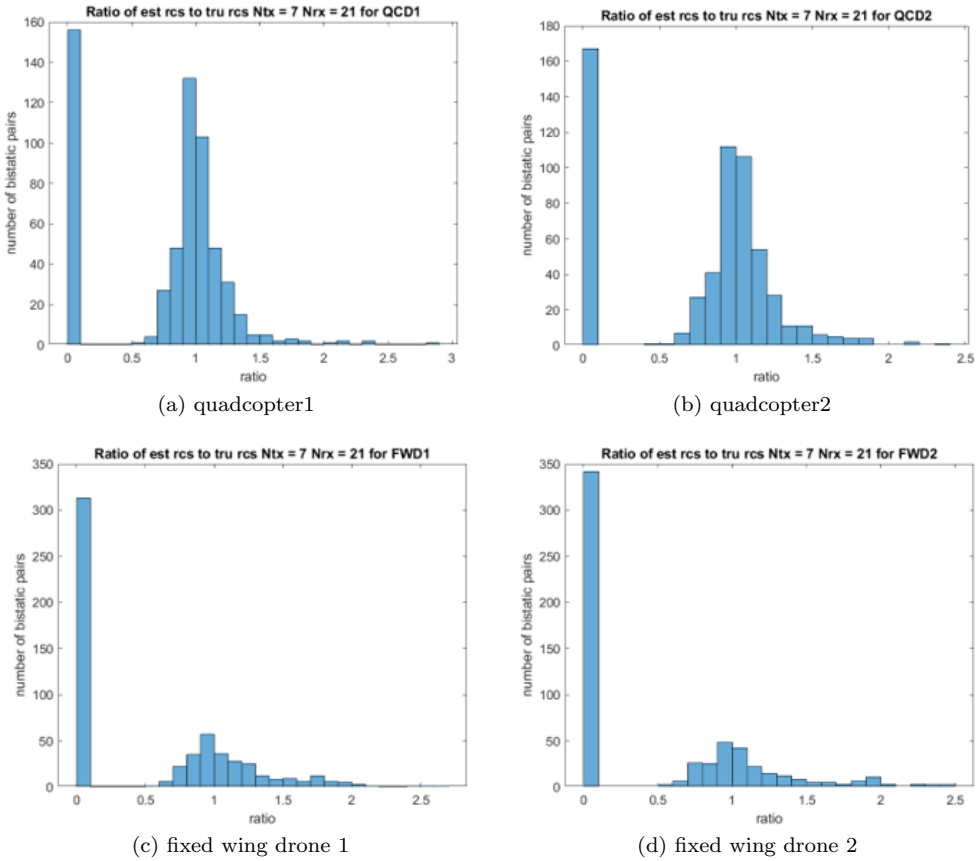


(a) quadcopter1

(b) quadcopter2

(c) fixed wing drone 1

(d) fixed wing drone 2

Figure 31: Histogram of ratio of estimated RCS to true RCS for different drones

### 3.6.2 Similarity Metric

Table 1 shows the error of the quadcopters and fixed-wing drones from their centroids. L1 error gives the best differentiation. The QCD1 and QCD2 drones have lesser error to the centroid of the quadcopters (MQCD) than the centroid of fixed-wing drones (MFWD). Similarly, FWD1 and FWD2 drones have lesser error to MFWD than MQCD.

| | MQCD | | MFWD | |
|---|---|---|---|---|
| Error | L1 | L2 | L1 | L2 |
| QCD1 | 917.41 | 281.76 | 1793.96 | 533.86 |
| QCD2 | 865.63 | 279.52 | 1613.49 | 498.80 |
| FWD1 | 1486.69 | 503.92 | 659.46 | 241.97 |
| FWD2 | 1139.42 | 424.82 | 556.05 | 202.96 |

Table 1: Similarity metric

### 3.6.3 Similarity Metric

In this similarity metric, there are two methods formulated. Metric1 calculates the mean error while the Metric2 calculates the noise standard deviation in both the cases. The results are shown in Table 2.

| | Metric1 | | Metric2 | |
|---|---|---|---|---|
| Error | QER | FER | QER | FER |
| QCD1 | 4.59 | 5.43 | 484 | 5.59 |
| QCD2 | 4.09 | 3.23 | 4.13 | 3.33 |
| FWD1 | 5.01 | 1.13 | 5.11 | 1.19 |
| FWD2 | 7.47 | 1.92 | 7.77 | 2.04 |

Table 2: Symmetric metric

As seen, for the quadcopter, both quadcopter error (QER) and fixed wing drone error (FER) are similar to each other (quadcopter has both ways of symmetry). For fixed wing drone, QER is very high compared to FER.

## 3.7 Conclusion

Thus the method developed uses the RCS measurements from a distributed radar system (bistatic RCS) to identify the type of drone, whether a quadcopter or a fixed-wing. Two metrics, Similarity and Symmetric metric are developed for the classification. Correct classification indicates the good accuracy of the metrics.

# References


1. McKeown, M.A. Cruickshank, David Lindsay, I.A.B. Farson, S.A.. (2002). Pilot-assisted channel estimation in MC-CDMA for future mobile cellular systems.

2. Raviteja, Patchava Phan, Khoa Hong, Yi. (2019). Embedded Pilot-Aided Channel Estimation for OTFS in Delay-Doppler Channels. IEEE Transactions on Vehicular Technology. PP. 1-1. 10.1109/TVT.2019.2906357.

3. M. Kanona, M. Hassan, and A. Abdalla, "Target classification in forward scattering radar in noisy environment," International Journal of Application or Innovation in Engineering Management, vol. 3, 11 2014.

4. S. Nambari, G. Rao, and K. Rao, Estimation of RCS for a Perfectly Conducting and Plasma Spheres, 12 2016, pp.437–447.

5. A. Register, W. D. Blair, L. Ehrman and P. K. Willett, "Using Measured RCS in a Serial, Decentralized Fusion Approach to Radar-Target Classification," 2008 IEEE Aerospace Conference, 2008, pp. 1-8, doi: 10.1109/AERO.2008.4526420.

6. Z. Mathews, L. Quiriconi, "Learning multi-static contextual target signatures," 2017 IEEE Radar Conference (RadarConf), 2017, pp. 1568-1572

7. J. S. Chen and E. K. Walton, "Comparison of Two Target Classification Techniques," in IEEE Transactions on AES, vol. AES-22, Jan. 1986

8. S. Roychowdhury and D. Ghosh, "Machine Learning Based Classification of Radar Signatures of Drones," 2021 2nd International Conference on Range Technology (ICORT), 2021, pp. 1-5, doi: 10.1109/ICORT52730.2021.9581973.

9. J. Mansukhani, D. Penchalaiah and A. Bhattacharyya, "RCS Based Target Classification Using Deep Learning Methods," 2021 2nd International Conference on Range Technology (ICORT), 2021, pp. 1-5, doi: 10.1109/ICORT52730.2021.9581336.

10. L. Xu, K. Zhan, H. Jiang, L. Bai and M. Wu, "Joint tracking and classification on aerodynamic model and RCS by ground-based passive radar," Proceedings of 2014 IEEE Chinese Guidance, Navigation and Control Conference, 2014, pp. 756-761, doi: 10.1109/CGNCC.2014.7007

11. S. Zhao, L. Zhang, Y. Zhou and N. Liu, "Signal Fusion-Based Algorithms to Discriminate Between Radar Targets and Deception Jamming in Distributed Multiple-Radar Architectures," in IEEE Sensors Journal, vol. 15, no. 11, pp. 6697-6706, Nov. 2015, doi: 10.1109/JSEN.2015.2440769.